10.1098/rsta.2001.0919

THE ROYAL SOCIETY

Ball lightning from atmospheric discharges via metal nanosphere oxidation: from soils, wood or metals

By John Abrahamson

Chemical and Process Engineering Department, University of Canterbury, Private Bag 4800, Christchurch, New Zealand

Published online 4 December 2001

The slow (diffusion-limited) oxidation of metal nanoparticles has previously been proposed as the mechanism for ball lightning energy release, and argued to be the result of a normal lightning strike on soil. Here this basic model of networked nanoparticles is detailed further, and extended to lightning strikes on metal structures, and also to the action of other storm-related discharges or man-made discharges. The basic model predicted the important properties of 'average' observed ball lightning, and the extension in this paper also covers high-energy examples of ball lightning. Laboratory checks of the theory are described, and predictions given of what conditions are necessary for observing ball lightning in the laboratory. Key requirements of the model are a sheltered region near the strike foot and starting materials which can generate a metal vapour under intensive heating, including soil, wood or a metal structure. The evolution of hydrocarbons (often plastics) along with metal vapour can ensure the local survival of the metal vapour even in an oxidizing atmosphere. Subsequent condensation of this vapour to metallic nanoparticles in networks provides the coherence of a ball structure, which also releases light over an extended time. Also discussed is the passage of ball lightning through a sheet of building material, including glass, and its occasional charring of flesh on close contact.

Keywords: ball lightning; metal nanoparticles; oxidation; lightning strike

1. Introduction

The phenomenon of ball lightning is sufficiently long-lived (more than several seconds) to make the 'chemical' theory attractive, where the mass of the ball is said to contain within itself sufficient chemical energy to supply the visible radiation. The problem has been to define which chemical change is in progress during the life of the ball. This paper generally follows Abrahamson & Dinniss (2000), who related ball lightning to a regular lightning strike, leading to a gas-filled network of *metallic* nanoparticles, which then oxidize with oxygen and water from the surrounding air. The range of starting materials is broadened here, from soil, or soil and wood, to also include metal and plastic or metal and wood. Also, discharges other than lightning are considered.

A number of compilations of ball lightning observations have noted the strong correlation with stormy conditions, and lightning strikes. For example, of 112 observations of ball lightning that Rayle (1966) documented, 91 appeared during a storm,

 © 2001 The Royal Society

and 62 of these appeared to follow a lightning strike to ground (it is, however, rare for the observer to see the strike close-up, and then see the ball appear from it—see two examples of this in Abrahamson *et al.* (2002)). Away from buildings, the material most commonly in the path of the lightning strike is a tree, and then soil, or plant material, which are predominantly mixtures of oxides of silicon, aluminium, and iron in decreasing amounts, together with carbon-bearing humic material. If one takes soils (or tree root next to soils) simply as a mixture of silica and carbon, then under such high-temperature treatment one would expect some reduction of the silica to silicon metal:

$$SiO_2 + 2C \rightarrow Si + 2CO. \tag{1.1}$$

This will be followed by subsequent oxidation using oxygen in the air:

$$Si + O_2 \rightarrow SiO_2. \tag{1.2}$$

The fine particulate form of the metallic silicon expected after such impulsive heating provides a fuel for the ball lightning phenomenon when it originates in the open, as outlined in § 2.

If the lightning strikes a metal structure (for example, an aircraft aluminium alloy shell), vaporization of the metal occurs, and again the resulting fine metal particulate form can provide a glowing ball lightning, as described in § 9, with energy given by a similar oxidation of aluminium:

$$4Al + 3O_2 \rightarrow 2Al_2O_3. \tag{1.3}$$

Again, the metal may be preserved unoxidized by the presence of hydrocarbons (e.g. vaporized rubber, plastics) during the condensation process.

2. Lightning on soil, forming silicon, and its oxidation

It is well known that lightning leaves solid tubular or lumpy residues (fulgurites) after interacting with sand or soil (Yavuz & Can 1999), which indicate that the discharge has penetrated beneath the surface, and that the material has been molten. Similar heating of silica and carbon in finely divided form by an electric arc is used commercially to produce metallurgical grade silicon. The thermodynamics of this process have been reviewed (Hutchison *et al.* 1988), as a function of temperature and C/SiO_2 ratio. Most soils have an organic C content of around 2–4 mass %, reaching up to 10% for high organic matter soils, or even to 20% for peaty soils. The silica content is often in the 20–35% range, depending on the basic rock from which it has been derived. Thus the molar C/SiO_2 ratio can range from 0.1 to around 1 for high organic matter soils. Vapour from partly vaporized soil is expected to have the C/SiO_2 ratio of the soil, or higher, because of the higher volatility of the C component. Hutchison *et al.* show gas phase equilibrium compositions for temperatures up to 3500 K at atmospheric pressure, for C–O–Si systems with varying C/SiO_2 ratios. Above 3000 K, Si vapour is dominant for a molar C/SiO_2 ratio of 2, with SiO vapour similar to Si in partial pressure for a ratio of 1.5. Thus many high carbon soils would be expected to yield a mixture of Si and SiO vapour on being heated by an electrical discharge. Any adjacent wood (e.g. a root) also heated would add to the C content. Any aluminium oxides in the soil may also react under similar conditions, yielding Al vapour.

The material left behind after a lightning strike on soil and a tree has been noted (Essene & Fisher 1986) to contain silicon metal. Analysis of the fulgurite from a large lightning strike showed 100 μm spheroids of silicon metal, with some metallic iron, preserved from oxidation in lumps of dark silicate glass adjacent to a charred tree root, along a 30 m line of fulgurite masses. It is of interest that wood and plant *dendritus* can have by themselves a C/SiO_2 ratio of around 2, coincidentally optimum for the reduction to Si by high-temperature processes.

Silicon and silicon monoxide vapour from such rapid heating would be expected to expand into the surrounding air, and then cool by radiation loss and contact with cooler gas, nucleating and condensing into small droplets. Small particles less than 100 nm in size are routinely made in quantities for industry by this same process of vaporization, rapid removal of the vapour from the heated area, and then rapid cooling (Siegel 1998). These 'nanoparticles' are commonly found in chains, more or less branched depending on conditions, thus forming a network of particles.

Aleksandrov *et al*. (1983) found such filamentary particle structures from exploding wires and condensing vapours, in the presence of electric fields. They proposed that ball lightning comprises such networks. They noted that the structures are invisible when cold, because the particles are too small (very much less than 1 μm) to scatter visible light. These ideas have been elaborated on by Smirnov (1987), but still without a clear proposal for the basic chemical reaction occurring within the network structure, regarded as necessary to emit light. Following a lightning strike on soil/wood, the proposal here is that the resulting particles are mixtures of silicon metal, and silicon carbide or oxides, with perhaps some aluminium and other metals and their oxides, depending on the original composition of the soil or woody material. Initially only the dominant component silicon will be considered, resulting in nanoparticles of silicon metal (these will in practice probably be mixed with silicon carbide, or silicon monoxide and dioxide, depending on the C/SiO_2 ratio).

The resulting small particles of silicon metal may be expected to oxidize rapidly due to their extensive surface. The rate of oxidation may, however, be controlled below that required for an explosion, by the production of an oxide layer on the surface, limiting the rate of diffusion of oxygen to the metal beneath, or diffusion of metal to the oxygen. Small particles of size 10–50 nm can have oxide layers up to 5–25 nm over the life of their oxidation. The oxidation of silicon surfaces has been studied in the laboratory, showing that both oxygen and water are active in oxidation. Whether oxygen or water dominates the rate depends on their partial pressures. We use the first-order rates of Deal & Grove (1963) and assume that the initial higher rates observed with dry O_2 (Massoud & Plummer 1987) do not apply when moisture is present. At a surface temperature of 1473 K, in air saturated at 20 °C with water, silicon will then oxidize at $0.11\ \mathrm{nm\,s^{-1}}$ with the water available, and $0.085\ \mathrm{nm\,s^{-1}}$ with the oxygen available. The early thin film oxidation rate is constant with time (Deal & Grove 1963) for thicknesses of silica layer of less than 100 nm, and will thus give an oxidation time of *ca.* $10\ \mathrm{nm}/0.1\ \mathrm{nm\,s^{-1}} = 10\ \mathrm{s}$ for the oxidation of a 20 nm particle of silicon at 1473 K. This is the correct order of magnitude for the radiative lifetime of many ball lightning observations.

The simple scheme of chemical reduction, particle formation and oxidation is shown in figure 1. This scheme involves a number of assumptions, which will be checked further.

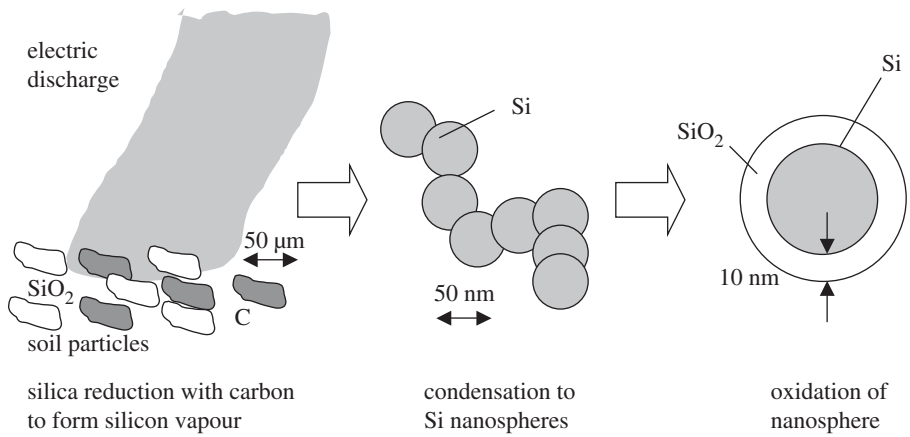

Figure 1. Formation of silicon-rich nanoparticles by lightning striking soil, followed by aggregation and oxidation.

1. Networks of nanospheres form when soil, or soil and wood is subjected to a high voltage discharge. If this does occur, does it occur at atmospheric pressure, and for typical lightning strike discharge levels?

2. 1473 K was used as the typical ball temperature. Why choose this arbitrary value?

3. A spherical assembly of particle strings forms from the vapour cloud. How does this fragile assembly form?

If a similar lightning strike vaporized a metal component (e.g. an aircraft skin), the metal vapour will in most cases be mixed by turbulence with the air, causing oxidation of the metal while in the vapour form. Then particles of the *oxide* are expected to nucleate, without the possibility of any slow oxidation of metal particles. If on the other hand, the metal is vaporized with a material which provides a hydrocarbon atmosphere (e.g. rubber, plastic, wood), then a similar reducing environment to that expected from soil and wood will persist for some time, allowing the metal vapour to cool unoxidized, and metal particles to form. If the metal vapour is not mixed with air or even with any associated hydrocarbon products (methane, carbon monoxide), then on cooling through the vapour-to-liquid transition the whole mass will contract, yielding a high concentration of metal in the resulting volume.

In the following experimental section, we show that strings of nanoparticles do in fact result from a lightning-like strike on soil samples at atmospheric pressure. The second and third points will be covered later in the discussion.

3. Experimental

A high voltage discharge through air at atmospheric pressure was used in a laboratory to simulate the last section of a lightning discharge in its interaction with the ground. Soil was placed in a 3 mm thick layer on a flat conducting (graphite) base below a vertical graphite electrode as shown in figure 2. A large capacitor was built up (maximum 204 μF), supplied with up to 20 kV DC potential (of either polarity),

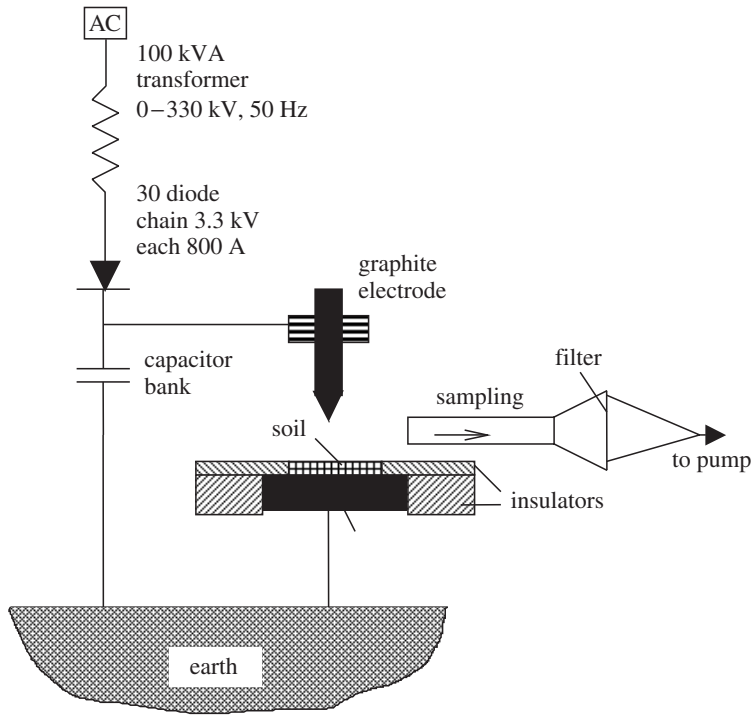

Figure 2. Experimental arrangement showing the power supply, electrode geometry and gas sampling.

delivering a maximum of 110 kJ across the air space above the soil. A gap of 22–36 mm was used, with breakdown voltages of 8–18 kV, and with charge transfer during the pulse of 1.3–3.4 C. The higher-power experiments used a negative polarity on the vertical electrode. For the highest power the capacitors were arranged in two banks in series, each bank consisting of 24 capacitors connected in parallel. The two runs reported below were run with the highest capacitance, with a gap of 22 mm, with 10.7 kV and 14.9 kV flash-over voltages for two silt loams (Takahe A and Tekuiti A soils respectively), resulting in 2.2 C and 3.0 C passed.

Sampling of the air space close to the discharge was done with a vacuum pump drawing air through a nozzle and across a fine silica fibre filter (Gelman A/E, glass), on the front of which was placed a nickel transmission electronmicroscope (TEM) grid. The sampling was carried out continuously before, during and after the discharge, until the area was made safe to allow turn-off. Subsequently, the deposit on the filter was examined by scanning electron microscopy (SEM) and the deposit on the grid was examined by TEM. Prior to the use of the filter, a single jet impactor was used to deposit expected particles. In spite of a jet velocity of more than 200 m s^{-1}, no deposit was ever found with this method.

One of the two soils used was finer and with more carbon than the other. The properties of the Takahe A and Te Kuiti A soils were, respectively, 3.0% carbon and 12.5% carbon; for the median (mass) particle size 13 μm and 5 μm; major mineral 70% mica and 100% allophane. For each run, the soil was poured into a circular cavity, 3 mm deep and 40 mm in diameter, in a 3 mm thick 100×100 mm^2 Bakelite

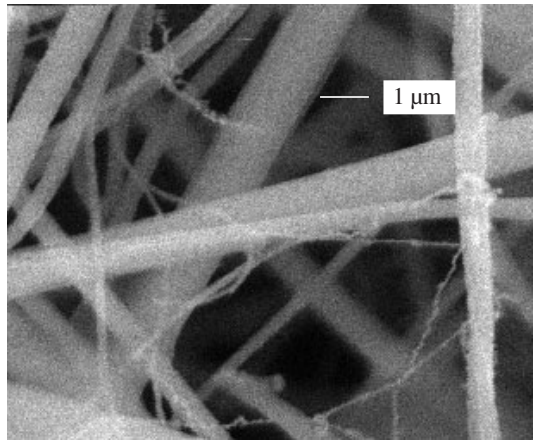

Figure 3. SEM of the deposit on silica filter fibres, after sampling the gas space above a discharge on Te Kuiti A soil, 14.9 kV flashover, 3.0 C. Note the lumpy character of the fine filaments.

plate, concentric with the point of the 15 mm diameter electrode above, and the soil scraped level and excess removed.

At the higher power levels, the soil sample was always completely blown away from the apparatus in the radial direction. Occasionally, the Bakelite surround which held the soil on the base was shattered and also travelled away some tens of metres. If the soil was dry, often it would 'fluidize' as the voltage was increased, and fountain up, emptying the cavity before flashover. If the soil was moist, this did not happen. At the higher-power levels, moistening the soil with one-third of its weight of water was necessary to retain it, and so have it there for interaction with the discharge. This was done for all the runs mentioned here.

The SEM was used to explore the filter samples to indicate which ones to study at higher resolution with the TEM. Control samples, taken without electrical discharge, were also examined to provide comparison with the run samples. One control was the clean filter, and the other the filter with soil on it (sampled by the vacuum pump from an air suspension of the soil). The clean filter showed only smooth fibres. Soil particles on the control samples were irregular and mostly greater than 10 μm.

Discharge experiments with the highest power showed fine filaments strung between the filter fibres, and even wrapped around the fibres, as shown in figures 3 and 4, for samples 27 (Te Kuiti soil) and 26 (Takahe soil) respectively. Viewed under the SEM, these filaments appeared lumpy with an average diameter of 100 nm and with lengths up to 7 μm. A higher number of these filaments was found for sample 26. Figure 4 also shows a larger sphere, of *ca.* 2 μm diameter. The TEM grid from sample 26 was examined under the TEM and found to be covered with fine strings of spherical particles, as shown in figure 5. The spherical particles ranged from 10 nm to 60 nm in diameter (average 25 nm), with their chainwidth in the interval 25–120 nm. No chains were found across the holes in the TEM (nickel) grid, but atomic force microscopy showed that the upper surfaces of the grid were covered in chains. Six of the highest power runs were examined with the TEM using three soils, and all but one showed similar chains of nanospheres; this exception showed only the larger particles. Images taken at the highest magnification appeared to show crystallites within the nanospheres.

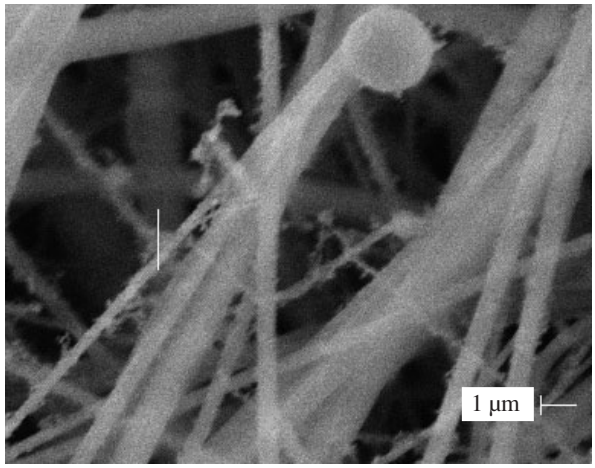

Figure 4. SEM of the deposit on silica filter fibres, after sampling the gas space above a discharge on Takahe A soil, 10.7 kV flashover, 2.2 C. The larger sphere was *ca.* 2 μm in diameter and had a smooth surface on closer inspection.

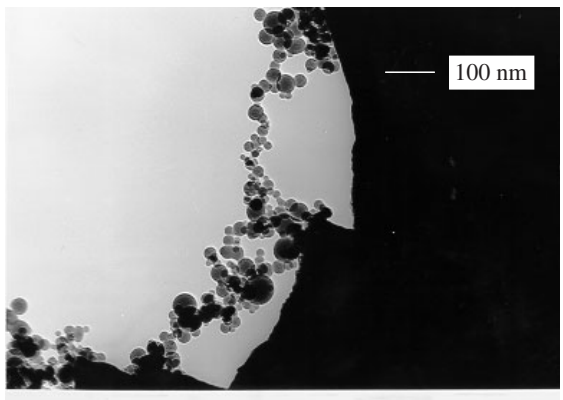

Figure 5. TEM of deposit on a nickel grid, from the same run as in figure 4. This shows the extended agglomerate character of the filaments, made up of nanospheres.

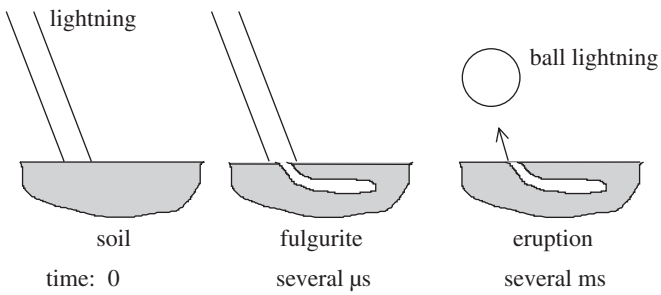

Figure 6. Depiction of ball lightning formation from a linear lightning strike, by formation of silicon and carbon bearing high temperature vapour within a fulgurite, followed by ejection into the atmosphere.

Air sampling was done at $20\,\mathrm{l\,min^{-1}}$, with the nozzle placed 40 mm from the discharge axis. The time for the air sample to reach the filter and grid from the nozzle is estimated as 50 ms, and the face velocity through the array of collecting fibres and grid was $0.30\,\mathrm{m\,s^{-1}}$.

An attempt was made to identify the composition of the particles with the SEM electron dispersive spectrophotometry (EDS) probe, but the fine filaments were not substantial enough to give a reading. Instead some larger spheres (one appears in figure 4) were analysed, and were predominantly Si, but showed by the varying (much smaller content) Al, Mg, Ca, Na and Fe readings that they were similar to the soil analysis. In contrast, the control filter fibre showed no Al, but much stronger Na.

4. Significance of the phase one experiments

The major result is the finding of strings of spheres with diameters in the tens of nanometres range, closely grouped on the surface of the TEM grid. No strings extended across the grid holes, probably indicating that longer strings were blown past during sampling. These nanospheres are likely to be the result of complete vaporization of soil particles with subsequent condensation. The larger spherical particles found by SEM, although less frequent than the filaments (identified as the strings of nanospheres), contained collectively at least as much mass. They contained largely Si, and appear to have passed through the liquid phase, whether as oxide (melting point 1980 K) or as metal (melting point 1680 K). It is probable that these much larger spheres did not result from recondensation of vapour, and are soil particles which have merely experienced melting. In that case, the analysis of them may not indicate correctly the composition of the much smaller nanospheres.

Energy passed to the soil particles from the discharge is expected to result from electrical breakdown within the gas cavities between the soil particles. Energy for heating the soil particles will come from the product (charge transferred) $\times$ (potential gradient within the soil). With the assumption that the voltage gradient will not be radically different between lightning and our experiments, our experiment was thus designed for lightning-like charge transfer rather than a maximum total discharge voltage drop (long path). It is therefore interesting to compare the charge transferred in these experiments with that estimated from lightning. The distribution shown by Rayle (1966) indicates that our maximum (3.4 C) is at the bottom 35 percentile of observed lightning strikes. In our experiments, the rise time was considerably shorter than natural lightning. Using a probe situated to record the field during the discharge, the peak was 10 ns after breakdown, with considerable slower ringing after that.

Thus despite having similar energy dissipation per unit depth of soil to many natural lightning strikes, we did not observe a coherent aerogel ball in our experiments, but observed the strings of nanospheres which could be its components. The dominant impression gained from the experiments was the severity of the shock wave, with consequent gas disturbance close to the discharge. The expanding shock wave which accompanies a lightning strike is expected to remove most vaporizing fine suspended matter from the discharge centre within milliseconds. Thus it is difficult to image a delicate network of particle chains being formed.

5. Lightning penetration beneath the soil surface

Andrianov & Sinitsyn (1977) have suggested that the glowing material of ball lightning is generated during the formation of fulgurites, i.e. during the lightning penetration and melting of soil beneath its surface. They did not have the idea of a particle network being formed, but recognized that the surrounding soil held the heated material together during the discharge. They simulated a fulgurite in their experiments by arranging a pulsed arc through tubes of various materials that eroded during the discharge, and evacuated the chamber before each experiment. The evaporated material was then initially without oxygen. The pressure rise associated with the evaporation then burst a thin polyethylene film acting as a barrier to the atmosphere. The hot material discharged through to the atmosphere, in the form of a luminous spherical ball, which then evolved further into an irregular or regular ring, depending on the geometry of the discharge nozzle. The inner linings used were made of ice or plastics.

They used an 80 μF capacitor bank, and charged this to 12 kV (delivering *ca.* 1 C of charge). They found luminous objects of a similar size (150–400 mm) to that reported for ball lightning. The energy use per gram of evaporated material was *ca.* 170 kJ g^{-1}. Their objects generally did not last more than a few milliseconds, and were much brighter than observed ball lightning. However, the eroded materials they chose (ice and plastics) did not contain metal in significant quantity, to allow subsequent condensation into fine drops, followed by a much slower film-limited oxidation as discussed above. The suspended carbon produced by the plastics is expected to oxidize within the several milliseconds observed for the luminosity (this is a characteristic oxidation time for 10–50 nm soot particles in a flame (Flagan & Seinfeld 1988)). The gas outflow under pressure through an orifice furthermore shows all the features of a 'vortex ring', the toroidal vortex formed by sudden discharge of a fluid through a circular opening (Shariff 1992; Johari 1995). Vortex rings are well known for retaining regions of their fluid with almost no mixing with the surroundings, for transport over considerable distances. In the pulse experiments (Andrianov & Sinitsyn 1977) sometimes secondary vortices formed. The appearance of the luminous ball was several milliseconds *after* the electrical discharge.

With the help of this experience, the possible chain of events leading to ball lightning becomes clearer, and is depicted in figure 6. After a lightning strike, the entrance to the fulgurite forms a natural nozzle for a momentary gas discharge via a vortex ring into the atmosphere. The likely temperature, velocity and pressure of this pulse of gas can be obtained from other reported experimental studies, as now discussed below. Some estimate of the energy involved will be useful for predicting experimental conditions for making ball lightning in the laboratory.

A first estimate of the energy required for producing a high-temperature vapour can be obtained from equation (1.1). Assuming the stoichiometry of equation (1.1), with solid SiO_2 and C at room temperature converted to Si vapour and CO gas at 3000 K, and using the enthalpies of formation listed in the JANAF tables (Stull & Prophet 1971; Chase *et al.* 1985), the required enthalpy change is 1066 kJ mol^{-1} of SiO_2, or 12.7 kJ g^{-1}. In practice, much of the energy of an electrical discharge through a powder (here soil) is expected to be taken by conduction and melting and we turn to experience with lightning-like discharges through soil-like materials. The mass of melted sand around fuselinks packed with sand after they have arced

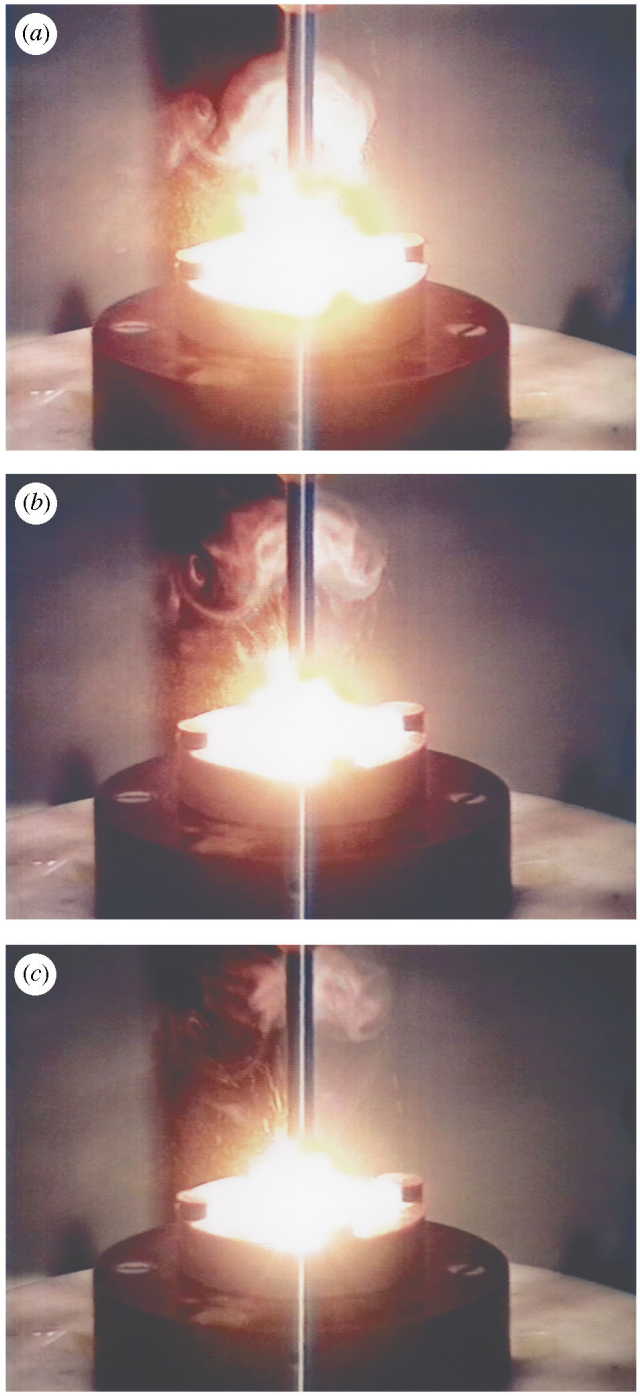

Figure 7. Successive video frames ($25\ \mathrm{s}^{-1}$) showing the rising incandescent vortex around the top electrode, after a 14 kV pulse discharge on a deep bed of Takahe A soil equilibrated with 100 % RH air (without carbon wick). A water resistor of 100 Ω was used, with the air gap 15 mm.

has been measured (Turner & Turner 1973). At lower arc energies, the melted mass was proportional to the energy of the arc pulse, with slope 2.1 kJ g^{-1} of the mass of fulgurite. This was found to equal that required for the heat-up of sand to the melting temperature plus fusion enthalpy. Thus in the time of the pulse, little energy penetrates beyond the fulgurite by conduction, and almost all results in melting. For higher energies, Turner & Turner found that increasing energy is required per mass of fulgurite, indicating that energy is also being used in vaporization. This occurs where the current density is greater than 10 A mm^{-2} (Stokes *et al.* 1989), based on tube area.

Yavuz & Can (1999) suggested that the lightning leader stroke from air to earth initiates the formation of a fulgurite channel, starting the fusing of wall material, and the following ground to cloud return stroke, which carries much more charge (e.g. several 100 A for several milliseconds) then vaporizes some of the soil on its passage through the same fulgurite channel. This latter step parallels experimental pulse discharges through tubes, which vaporize the walls, called 'ablation arcs'. Stokes *et al.* (1989) have studied the mass ablated from the walls of such pulsed (several milliseconds) ablation arcs and have developed a model describing the energy and mass flows. Their tubes were of similar size to natural fulgurites (6–20 mm in diameter), but only 75–150 mm long and were made of a number of different materials, including plastics. From their experiments they found that rates of mass loss averaged over the pulse were almost linearly related to the peak power, so that one can estimate approximately the total energy used in vaporization. This amounted to 30–50 kJ g^{-1} of ablated material, for a range of plastics (considerably lower than the 170 kJ g^{-1} of Adrianov & Sinitsyn (1977), possibly because of the longer tubes). The heat-up plus vaporization enthalpy for these materials was in the range 4–12 kJ g^{-1} and much less than the total energy dissipated.

Factors which are of interest here are the pressure build-up in the tube farthest from the open end (up to 100 bar for the highest current density), and the resulting axial flow pulse which reaches sonic velocity just before exhausting to the environment. The controlling flow of energy appears to be radiation from the arc core to the ablating wall (Stokes & Cao 1989). For plastic materials, an optically dense cloud of carbon particles formed close to the wall, between the arc core and the wall, which interfered somewhat with this radiative transfer. The axial exhaust jet temperatures were in the range 2500–3500 K, and the exhaust had a 'bell-like' structure (Stokes & Cao 1989), indicating perhaps a barrel shockwave. The wall materials used were with one exception coherent and sufficiently strong that the highest wall shear did not remove material. The same would not be the case with soil, and removal of some soil particles with the emerging jet is expected.

To get some idea of how natural lightning compares with these experiments, one can use an assessment of the minimum breakdown gradient of lightning through soils (Mousa 1992), applicable to paths of greater than 0.5 m in length. His value of 50 kV m^{-1} appears to correspond to normally moist soils, and likely also for developed fulgurite/arc conditions. This voltage gradient corresponds to a potential difference of 3.5 kV over the 75 mm long tubes of Stokes *et al.* (1989), which is greater than their highest value. Their data show increasing functions of voltage and also pressure as a function of current density and from their data one thus expects more than 300 A mm^{-2} (their limit) for current density for lightning in a natural fulgurite, and more than 50 bar for pressure.

Lightning strikes on trees have formed furrows in the soil between the struck tree and neighbouring electrically grounded conductors. This presumably occurs where the path has remained close beneath the soil surface, so that upward expansion of the vapour generated along the lightning path drags the soil out with it. It is not uncommon that these furrows are 20 m long (Mousa 1992). If the path is deep within the soil, the vapour cannot be released so easily laterally, but can be released at the path ends (at the lightning foot, and where the path attaches to a conductor).

This description can be compared with observed behaviour of lightning strikes where the strike was triggered by a rocket probe (Fieux *et al.* 1975), so that both the time and location of the interaction with the ground was known. Beads of luminosity *ca.* 400 mm in diameter were observed to form from distortions of the linear lightning near the ground, and these were interpreted as 'bead lightning'. What is of most interest here is that several similar luminous objects (lifetime several tenths of a second) were also seen at the base of nearby wooden posts. This suggests that hot vapour escaped from the other end of an extended lightning subsoil channel reaching the posts, probably spanning the 4 m distance between the bottom of the rocket launch pipe and the posts. The latter are expected to act as electrical earth as they would have been set into the ground by at least 1 m, and would likely have been impregnated with salts for long life.

The temperature of vapour resulting from ejection from a fulgurite of melting soil can then be estimated. The enthalpy change estimated above for a SiO_2/C mix ($12.7\,\mathrm{kJ\,g^{-1}}$) is within the range observed in the above ablation arcs for plastics (4–$12\,\mathrm{kJ\,g^{-1}}$). If no erosion of soil particles occurs, the temperature at the mouth is then expected to be in a similar range to that found with the plastics above, i.e. 2500–3500 K, or a little higher, accounting for the higher current densities mentioned above. Two factors will make the actual temperature of a ball formed from the fulgurite jet less than these figures. First, erosion of the wall of the fulgurite will introduce cooler soil particles into the vapour jet. Second, the fluid making up a vortex ring largely comes from the boundary layer within a vortex generator (Johari 1995) so the cooler flow close to the wall of the fulgurite (containing most of the erosion material) is expected to be fed into the developing ball. The amount of eroded soil will depend on the properties of the soil, and is difficult to estimate. High current lightning pulses which achieve high pressures deep within the fulgurite, and sonic velocity at the mouth, also will have a shock wave over the mouth flow, which will interfere with development of a coherent ring vortex and ball.

6. Further experiments related to the fulgurite mechanism

The importance of momentary shelter for the condensing and aggregating particle chains prompted later experiments where small fulgurites were formed. The soil bed was deepened and narrowed, with insulation provided on the upper bed wall to ensure arc penetration only through the soil before termination to the lower conducting wall. Similar energies, voltages and charge transfers were used as before. Small fulgurites were formed, of dimensions 1–2 mm × 10 mm, with coherent walls of thickness *ca.* 0.5 mm. The whole soil bed would often erupt, apparently from vapour being formed near the bottom of the bed where the arc crossed to the wall electrode. To avoid this, and to simulate the later longer lightning strike through an existing fulgurite (Yavuz & Can 1999), a graphite base was placed under the bed and a fine

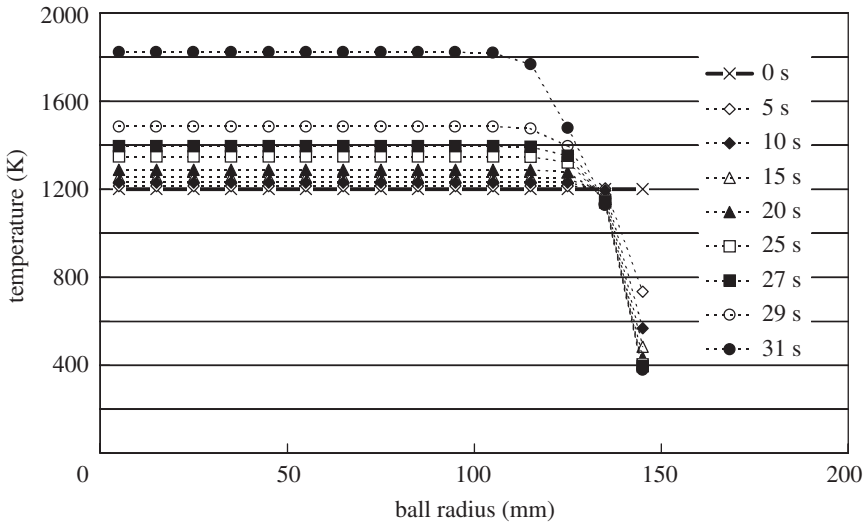

Figure 8. Nanoparticle ball model prediction of internal temperature profiles at different times, for a 300 mm diameter ball lightning, with a reactive silicon loading of 100 g m^{-3} (of 25 nm particles), unreactive oxide loading of 800 g m^{-3}, and an initial temperature of 1200 K.

graphite rod (0.3 or 0.5 mm diameter pencil lead grade B) was inserted through the bed until it touched the base, with a few mm left exposed at the top. Also, to simulate this longer strike, resistances with values from 30 Ω to 920 kΩ (cells containing salted water) were added in series with the arc gap, extending the discharge time. Discharge times with 30 Ω were 4 μs, and with 800 Ω, 8 ms. Again, the soil fountained off if dry, and to avoid this was generally previously wetted by leaving it in air of 100% RH for several days. Some wood dust was occasionally mixed with the soil.

No coherent ball was formed from these experiments, but from video recordings hot (emitting) material was observed in a ring vortex formation rising symmetrically around the top graphite electrode, as shown in figure 7. This top electrode had been reduced in diameter (to 8 mm) and lengthened to *ca.* 100 mm from its larger diameter support to minimize interference, but it may still have interfered with the formation of a ball. These eddy structures were observed in only two runs from a series of 24 during the year 2000. It may be significant that these appeared at an *intermediate* power level at the shortest pulse time. Many small white spheres (visible to the naked eye) were found within the soil around the fulgurites, on top of the soil, and stuck to the upper electrode, which was in line with the ejected pulse. For the longer pulse times, sampling showed many 5–50 nm diameter fibres on the TEM grid surfaces, along with deformation and cracking of the nickel grids. It was apparent that the nickel had heated during the sampling of the discharge gases and oxidation had occurred. The previous samples of short discharges showed no such grid attack.

It can be noted that no double strike was attempted, so that the path of the arc was always cold at the start of these pulse experiments. The higher-energy experiments are likely to have had sonic velocity at the mouth of the fulgurite, and thus severe distortion by the shockwave of any developing ring vortex.

7. Aggregation of particles into chains and into a ball

We have to ask how particle chains can form, and what conditions are necessary for them to build to a large assembly?

Abrahamson & Marshall (2002) have reviewed the aggregation of particles into chains, including those from slightly oxidized metallic nanoparticles, arguing that the observed open chain structures (fractal dimension between 1 and 1.8) come from directed electrical dipole-to-dipole additions, using the attractive force of permanent dipoles. For the metal nanoparticles, these dipoles are produced by fixed charges near the internal interface between the metal core and the oxide coating. In order to build chain structures longer than *ca.* 1 mm, Brownian diffusion is inadequate by itself to bring the larger agglomerates near each other, and a mild turbulent mixing is necessary, with its much larger scale of diffusion. For the dipole–dipole interaction to be effective, the concentration of gaseous ions must be sufficiently small to avoid Debye screening of the local dipole fields. The temperature for aggregation is thus limited to less than 2000 K (Fortov *et al.* 1997). Below the melting point for silicon (1680 K), the particle oxide layer is expected to be stable, and chains that develop will have some strength due initially to dipole–dipole attraction.

Some protection from immediate mixing with oxygen or water vapour is needed during this aggregation into a stable network. As noted above, the fluid dynamics of a vortex ring is ideal for this. Once the network has formed with the help of mild turbulent motion, the gas within the ball is likely to be further isolated from mixing with the surrounding air, by coherence of the outer layers. Destruction of the fine network by sintering to make a much smaller number of larger particles is very much a possibility. Metal nanoparticles sinter easily, even at room temperatures, if there is no oxygen present (Olynick *et al.* 1996). However, in the normal environment containing a trace of oxygen they quickly build a slight oxide coating and stabilize as nanoparticles. We must then look at the sintering behaviour of the coating at higher temperatures. Taking SiO_2 as our example, the sintering time τ_f of SiO_2 spheres (Xiong & Pratsinis 1993) is of Arrhenius form,

$$\tau_\mathrm{f} = 1.3 \times 10^{-14} a \exp\left(\frac{8.3 \times 10^4}{T_\mathrm{p}}\right), \tag{7.1}$$

for radius a in centimetres, and temperature T_p in kelvin, giving τ_p in seconds. For a 25 nm SiO_2 particle, τ_p becomes 10 s at a temperature of 1730 K. Thus if the (coated) particles are brought rapidly below *ca.* 1700 K, they are not expected to sinter together in the lifetime of the ball, and thus the nanostructure will be stable against surface tension effects.

8. Modelling of a silicon metal aerogel ball after formation

The model of oxidation presented in § 2 depends on the oxidation of a single nanosphere of silicon to characterize the lifetime of the ball lightning. It is more realistic to model the whole ball of networked nanospheres.

An estimation is given in Appendix B *c* of the cooling of an individual Si or SiO or SiO_2 nanosphere, indicating that radiation is not important, but thermal conduction with the surrounding gas is (a very much less than 1 K hotter particle is necessary to lose the heat of reaction to the gas). A reference point for our model is that of

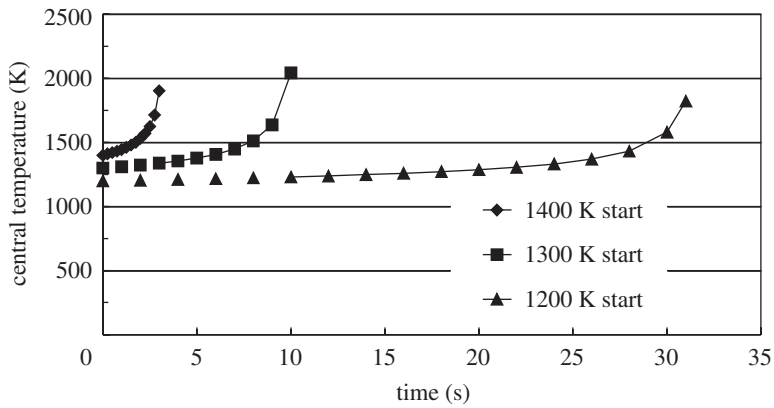

Figure 9. Ball lightning central temperatures predicted from the particle network model with parameters as in figure 8, for starting temperatures 1200, 1300 and 1400 K. Lifetimes before melting are *ca.* 30, 10 and 3 s, respectively.

a stagnant (non-mixing) sphere of air either pure or lightly loaded with particles (Lowke *et al*. 1969). For a ball of 400 mm diameter they estimated a characteristic time of tens of seconds to cool from 3000 K (uniform) to 1000 K. However, such a hot sphere without some coherent force is not expected to stay unmixed for so long because of buoyancy currents in the air outside it, causing movement within the sphere via shear at the perimeter.

In the model presented by Abrahamson & Dinniss (2000), turbulent or convective mixing *within* a network of particles is assumed negligible. In support of this, an estimation in Appendix B *b* of drag between included gas and a network of the chains indicates that this mix is almost inseparable, and the network will carry the gas with it wherever it deforms. This framework is expected to develop first at the cooled perimeter of the vapour cloud, providing a laminar buffer to turbulent mixing with the surrounding air.

The transient (symmetrical) temperature profile of the resulting ball can be evaluated from energy conservation for a thin shell of the ball between radius r and $r+\delta r$ over a time-interval δt,

$$(\rho C_{\mathrm{p}})_{\mathrm{ball}}(4\pi r^2\delta r)\delta T_{\mathrm{rise}} = [-\delta(4\pi r^2 q) + H(4\pi r^2\delta r)]\delta t, \tag{8.1}$$

where the thermal flux q is given by $q = -k\delta T/\delta r$, and k, ρ, C_{p} are thermal conductivity, density and specific heat of the ball; H is the rate of heat evolution per unit volume. Equation (8.1) was integrated in a spreadsheet with property values derived from the assumptions listed below. Temperature profiles at various times are shown in figure 8 for a ball of 300 mm diameter, beginning at a temperature of 1300 K throughout, and with a reactive concentration of 100 g Si m^{-3} (see assumption 1 below) formed from 25 nm diameter nanospheres. It can be seen that the interior of the ball is not affected by heat losses from the surface over the likely life.

Figure 9 shows the central plateau temperature with time for various starting temperatures. The effect of the increasing oxidation rate with temperature is to rapidly increase this core temperature after a certain time. This time depends on the starting temperature, being *ca.* 3 s for 1400 K and 30 s for 1200 K. Thus this model predicts a violent end to the ball because as the temperature rises above

1700 K or above 2000 K, silicon particle cores, or silica coatings, respectively will melt, increasing the possible oxidation rate, and reducing network strength. For lower reactive metal loadings (e.g. for low carbon soils), however, the ball temperature may not reach the melting temperature, and the ball is then expected to fade from view as it cools. For low starting temperatures, because much of the material may not scatter light, and is not hot enough to emit appreciable radiation, the ball may become visible only over the later part of its lifetime, which could be after minutes, so that it is then not easily connected with the originating lightning strike. To the observer, it has then 'appeared out of thin air'.

Assumptions made in the model are as follows, with justifications given previously or in the appendixes.

1. The silicon/silicon monoxide content was estimated from equilibrium vapour concentrations (at 1 atm pressure, exiting the fulgurite) in the range 3000–5000 K for starting materials with C/SiO_2 ratios those of soils, and for pressures close to atmospheric. This results in *ca.* 100 g m^{-3} of particulate Si and SiO combined (see Appendix A *a*). The fast condensation is expected to give Si and SiO particles and CO as the main gas component. Some carbon may also appear along with a hydrocarbon content, with SiC appearing slowly at lower temperatures, but the effect of these is not included in the model results in figures 8 and 9. The total solids content (including non-reactive solids eroded from the walls) allows for *neutral* buoyancy (many examples of ball lightning move neither up nor down). This results in a total solids content of *ca.* 900 g m^{-3} (see Appendix A *a*).

2. The small size and high number of particles in the network structure within the ball prevents bulk motion of the trapped air relative to the network, allowing only diffusion and thermal conduction (see Appendix B *b*).

3. Radiation from the nanospheres, while probably important for making the ball visible, and determining the colour, does not significantly affect the energy balance of the ball (see Appendix B *c*). Carbon (soot) has a much higher emissivity, but has not been considered because if it is produced it will be removed quickly by combustion. This will simply alter the starting temperature of our model, which applies to the slow combustion of the remaining metal/oxide particles.

4. Energy loss is by conduction within the ball, and then from the exterior of the ball by natural convection (buoyancy losses, see A *c*). The conductivity contribution from the solids is ignored, because of the small content of *connected* solids (those in the network).

5. Energy dissipation within the ball depends on the surface area of the nanospheres (i.e. on their size and number) and on the temperature. The rate of reaction can be taken from the measurements on planar surfaces of silicon under atmospheres of oxygen and water vapour, for the linear period of oxidation (less than 100 nm thickness) (see Appendix A *b*).

6. The rate of reaction and thus H is not limited by diffusion of oxygen into the ball (see Appendix B *a*), i.e. gas oxygen mole fraction remains constant at all radii (this is an excellent approximation for $T < 1400$ K).

The above assumptions give rates of external energy loss by convection of 20–40 W for a 300 mm ball once the inner temperature reaches *ca.* 1450 K. The rates of energy release are much higher than this (here 1.1 kW), and this release is mostly absorbed by heating the ball mass. The total chemical energy is 3.3 MJ m^{-3}, lying within the very approximate observation estimates of 1.5–15 MJ m^{-3} for 'average' ball lightning (Smirnov 1987).

(*a*) *Other predictions from the soil model*

1. There is a narrow window of C/SiO_2 ratios for Si condensation of 1.2–2.0 (Hutchison *et al.* 1988); below this, SiO_2 condenses (for equilibrium conditions), and above, SiC will deposit. However, for rapid condensation of SiO vapour, amorphous solid SiO is formed (Palik 1985). If SiO_2 particles are fully vaporized in an electric discharge in the absence of oxygen, a brown SiO aerosol appears to form (Gans & Gauvin 1988). If SiO nanospheres are formed from a lightning strike, the subsequent oxidation of them could be similar to that of silicon (Massoud 1995), with about 0.5 of the heat of oxidation (Nagamori *et al.* 1995).

2. For lower concentrations of reactive material, the life of the ball will not terminate with an eruption, but will fade by cooling from the outside. About 40% of observations of ball lightning do not end violently (Smirnov 1987). The violent end may be enhanced by disruption of the oxide layer around each particle when the oxide melting temperature is reached. If the reaction is almost complete when the temperature has reached that for rapid sintering (1700 K for silica, see above), the whole ball will rapidly collapse to nodules, as observed for some balls.

3. The colour and luminosity of the ball may depend on molecular emission from the vapour of salts present in the soil, but also on thermal emission from the nanospheres themselves. The simplest assumption is that the nanospheres emit or absorb according to the temperature of the ball, and according to optical properties of *bulk* materials. This latter is adequate for particles greater than 10 nm in diameter (Littau *et al.* 1993). Rayleigh's approximation (Bohren & Huffman 1983) for the absorption cross-section of a sphere allows one to estimate the linear absorption coefficient α_{abs} of the nanosphere suspension for various wavelengths, using listed values of extinction coefficient k and refractive index n for crystalline Si, crystalline SiO_2 and amorphous SiO (Bohren & Huffman 1983). For 100 g m^{-3} Si in the form of Si, SiO or SiO_2 the ball is optically transparent in the visible (e.g. for Si, at 600 nm wavelength, α_{abs} is 0.26 m^{-1}, so the optical thickness $\alpha_{\mathrm{abs}}D = 0.08 \ll 1$), allowing one to sum the contributions of all nanoparticles for the ball emission. Emissivity is taken as equal to absorptivity.

   The emission is the product of emissivity ($\propto k$) and the black-body emission e_{b} for each wavelength λ, giving a sharp peak in the red for both Si and SiO because $\mathrm{d}k/\mathrm{d}\lambda$ is negative and counters $\mathrm{d}e_{\mathrm{b}}/\mathrm{d}\lambda$ positive. Figure 10 shows this peak. At 1200–1400 K, 4.5–35 W is emitted from the whole Si peak, corresponding to 1.2–14 W over the *visible* range 400–800 nm. A 100 W tungsten filament lamp (observed ball lightning median according to Rayle (1966)) emits 8 W in

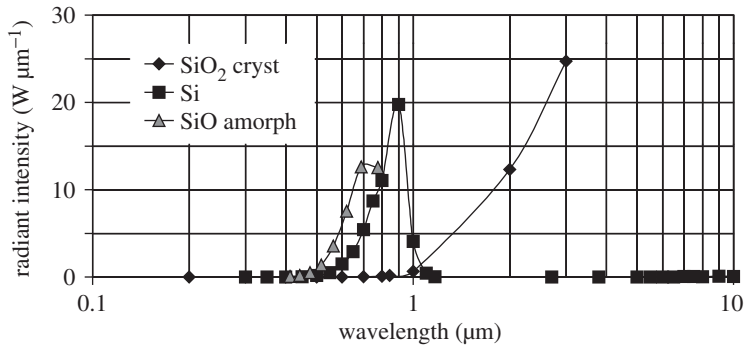

Figure 10. Radiant intensity of a 300 mm diameter ball lightning for a uniform temperature of 1200 K, accounting for 100 g m^{-3} of 25 nm active silicon-bearing particles, in the form of Si, SiO and finally SiO_2.

the visible (at 3000 K), well within the range expected from the model. The λ dependence of Si emission at 1200 K matches a 1700 K black-body profile in the visible, so would be reported as translucent white. Lower temperatures may be reported as yellow or red, thus covering the majority of observed colours. Other sources may be molecular emission from the vapour of salts present in the soil (e.g. green for copper). A blue halo around the ball is often reported, and this is expected to be from corona discharge at the electrically charged surface.

4. Electrical charging of the particles in the ball is expected (Smirnov 1987). The repulsion of like charges at the surface will give a restitutive character to the ball, bringing it back close to a spherical shape after deformation against solid boundaries.

5. A cool outer surface and lack of impression of (radiant) heat are natural outcomes of the model, corresponding to generally observed properties of ball lightning (Turner 1994).

6. The model does not account for the small number of balls seen originating from clouds or from lightning in the sky, unless the lightning comes across a body containing carbon and metal in its elemental composition. One such body is a large insect or a bird, as suggested by Fischer (1981).

9. Lightning and other discharges on metals

Lightning strikes on metal structures are also expected in some situations to result in a ring vortex, containing the metal vapour. The vaporizing channel need only be a few millimetres in diameter, and could form along the interface of a metal body and a hydrocarbon (e.g. plastic, rubber seal on an aircraft door (Pitts & Fisher 1988)). From the discussion in § 5, pressures of many bar are expected in such narrow channels, so that ejection of vapour into a 'pressurized' cabin (1 bar) is to be expected (this penetration may also occur through a seal in a bulkhead—see § 1 *t* in Abrahamson *et al*. (2002)). The hydrocarbon vapour from the seal will capture much of the

oxygen, preventing initial oxidation of the metal vapour, and so allow formation of metal nanoparticles on cooling. Once a network of these is formed into a ball, it is expected that the ball will be convected by the air ventilation flow (normally in commercial aircraft this is from front to rear), corresponding to the observed movement direction of ball lightning in aircraft.

Lightning punctures of the aircraft skin (Brick 1968) is damage more visible than puncture of a seal, which will self-seal and not be noticed. Often pressures of several bars are generated in the lightning channel itself (Lee 1986), which can provide the driving force for a gas jet through the hole into the aircraft cabin. Thus a ring vortex containing the metal vapour may also form in the space behind the skin. However, there is no carbon competing for the oxygen in this situation, and so metal nanoparticles are unlikely to form and hence ball lightning is also unlikely.

There are a number of laboratory pulse discharge experiments with both metal and hydrocarbon present (Bychkov 2002, this issue) which produce small ball lightning-like luminous bodies and can also be interpreted in the manner of this paper. Similar jet impulse flows may also occur with man-made electrical discharges (e.g. from faulty cabinets around switchgear). In some special geometries, the lightning channel will contact only metal, and thus pure metal vapour may be ejected to form a cooling cloud with little accompanying air. As outlined in § 2, this cloud will contract with the phase change to liquid or solid, leaving a high concentration of metal particles. This is expected to lead to a high-energy ball lightning. Interpretation of high-energy observations is further discussed elsewhere in this issue (Bychkov *et al*. 2002).

Many ball lightning appear without visible connection to a lightning strike, but during a thunderstorm. One possibility is the sudden release of a large charge induced by the storm field (Goodlet 1937, p. 10) on man-made metal bodies with large capacitance such as aerials, electric wiring, fencelines, roof cladding and underground piping. If these bodies are unearthed or poorly earthed, the pulse will occur when the most conducting route to earth suffers breakdown, e.g. an earthing fastening to a lightning conductor through a paint layer. The electrical pulse discharge of the release could act in a similar fashion to the more visible lightning. Section 1 *s* (Abrahamson *et al*. 2002) appears to be the result of such a discharge of limited stored charge on an aerial.

10. Self-luminous metal bodies

Aggregates of metal nanoparticles are routinely observed to heat by oxidation to become self-luminous, and this is discussed elsewhere in this issue (Merzbacher 2002). For example, samples of tungsten ultrafine powder initially at room temperature achieved red heat after a few seconds of exposure to air (Lamprey & Ripley 1962). The room temperature kinetics of oxidation are much faster at the same temperature than the high-temperature kinetics used in the model in § 8, and apply only for the first few layers of oxide (Fehlner & Mott 1970). Some of this covering will already be on most nanoparticle samples, scavenged from trace amounts of oxygen in the manufacturing environment. It is apparent that for some metal samples, the remaining initial oxidation when exposed to air heats the sample sufficiently for other higher temperature processes to become appreciable. One of these is likely to be the annealing of crystalline defects within the metal. Nanoparticles in kilograms quantities are being produced by the action of high pulse currents through fine wires in the absence

of oxygen (Tepper 1999), and many show a self-heating step to their melting point when first warmed (e.g. self-heating from 200 °C to 900 °C), attributed to defect annealing. At this higher temperature, the high-temperature oxidation kinetics are then expected to sustain the high temperature and thus luminosity.

This industrial experience of self-luminosity of metal nanoparticles thus supports the model put forward here for ball lightning, especially when it is applied to the direct vaporization of metals, and where the metal concentrations are high. For ball lightning it is unlikely that the lowest temperature before oxidation begins is as low as room temperature.

11. Interaction with water-containing substances and glass

Water is a reactant with most metals, and heat release from contact of ball lightning with water is expected, as discussed in the high-energy paper in this issue (Bychkov *et al.* 2002). Thus good contact of a high concentration metal ball with animal or human tissue is also expected to cause burns by oxidation, as seen in case A *i* in the observations paper in this issue (Abrahamson *et al.* 2002), where the contacted arm of a person became charred and black. Good contact with such a ball is expected to result in the metal particles heating the tissue, and progressing into the charred remains. Extensive contact with a high-concentration ball could provide an explanation for so-called 'human combustion' cases. Poor (e.g. glancing) contact is expected to result in little heat transfer from the cooler outer layers.

The passage of ball lightning through glass panes poses a difficult problem for most theories of ball lightning, and is said to be impossible for particulate/chemical theories. However, when the charged ball comes in contact with a pane with a moisture film (earthing film) on the other side, the high potential difference across it could cause electrical breakdown of the glass. There is considerable evidence for high charge on some ball lightning, and it is reasonable that the hot nanoparticle network could sometimes charge to the limit of electrical breakdown of the surrounding air. In this case, a corona discharge would be seen at the perimeter, corresponding to the observed blue halo seen around some balls. For this limit, the field at the perimeter E_0 will be that of air breakdown (3.3 kV mm^{-1} for a 200–300 mm diameter ball (Pedersen 1989)). For charge Q evenly distributed over the ball, the field E exterior to the ball at radius r is given by (Jackson 1975) in SI units

$$E = \frac{Q}{4\pi\varepsilon_0 r^2}. \tag{11.1}$$

Thus applying this at the perimeter, where $r = R$,

$$Q = 4\pi\varepsilon_0 E_0 R^2. \tag{11.2}$$

Substituting for Q in equation (11.1) and integrating E from infinity to R to obtain the potential V_0 at the ball surface,

$$V_0 = E_0 R. \tag{11.3}$$

Thus for a 300 mm diameter ball, $V_0 = 500$ kV. This is sufficient to break down a pane of glass. For example, a pane of borosilicate glass of 5 mm thickness requires *ca.* 90 kV for electrical breakdown (Clark 1962).

The ringing which has been heard during ball penetration (Grigor'ev *et al.* 1992), and in one case several short bursts of sound, are reminiscent of the observed pulsed breakdown of brittle solids by applied high DC fields (Andres & Timoshkin 1997) (caused by the 'tree' of fine discharge channels progressing in stages). Some panes are left with an opaque circular region where the ball travelled through, while others show no visible alteration. The opacity indicates boundaries which are large enough (*ca.* 1 μm) to scatter light. An extreme example of this is the 1758 laboratory observation of Arden & Constable described by Turner (2002), where 'a circle as white as chalk' remained after penetration of a small ball through a glass jar, and 'upon touching the white part, it dropped out, and appeared to be glass in a fine powder.'

If the primary chains (of several micrometres in length; see § 3) can be detached from each other, they will tend to migrate under the electric field through any such connected channels to the other side of the glass, and there possibly rearrange under the penetrating field of the ball. If there are pores smaller than scattering size, nanoparticles should still be able to travel through them, thus explaining the lack of visible change in many cases. Other examples of ball penetration show a clear break in a ring, which may result from the sharp change in temperature associated with the surface heating (this mechanism was suggested to the author by S. Singer (2001, personal communication), based on his similar industrial experience with glass).

Sheets of other building materials (wood, plaster) have been easily penetrated by ball lightning. These already have a porous structure and a similar electrical breakdown mechanism could link the pores to provide clear channels through to the other side. It is clear that an experimental testing programme is required to check these suggestions.

12. Physical and chemical requirements for generation of ball lightning

According to the theory presented in this paper, the first requirement to generate a long-lasting radiating ball is that metal vapour is produced by application of some energy at high temperature. This may be from an electrical discharge, or electrical resistance heating, or perhaps by frictional heating, as in earthquake fractures. The metal vapour may come directly from solid metal components, or by chemical reduction as in the heating of soil by a lightning strike. The second requirement is that the oxidation of this vapour should not compete strongly with its condensation and solidification into nanoparticles. Oxidation of the vapour will occur quickly at high temperatures in the presence of oxygen, so generally some carbon must be also present to convert any oxygen mixed into the vapour to carbon monoxide (the presence of merely hydrogen will result in water vapour and reaction with the metal). This requirement means that even with the vaporization of metal into air, some carbon is also necessary. This condition may be met in a lightning strike on an interface between metal and a hydrocarbon polymer (e.g. at a rubber door seal, or at the joint between a polymethacrylate window and metal frame, on an aircraft). The high latent heat released during condensation can tend to delay the cooling process, so a rapid removal of heating and a removal of the vapour from the heating area is helpful. Thus a pulsed input such as a pulsed electrical discharge appears optimum, also generating an expansion of vapour to other cooler regions.

A small amount of oxygen is required after particle formation, to thinly coat each particle with an oxide layer, to prevent sintering (merging) to much larger particles, and also to provide fixed charges making up electrical dipoles, so causing chains of the particles to form. This chain aggregation requires a low gaseous ion concentration to avoid their screening of dipole–dipole interactions, so easily ionized species such as alkali metals should be at low concentration and/or temperatures should be low (say, less than 1800 K) for some time before oxygen diffuses in or is mixed in. This time must be at least 1 s for Brownian motion producing chains of *ca.* 1 mm in length. For larger structures some mild turbulent mixing within the nanoparticle suspension is necessary to bring the longer chains together. This will naturally occur with flow situations such as those from a fulgurite or from a channel formed in a door seal.

Finally, the developing fragile structure of particle chains cannot be exposed to violent shearing flows, intensive turbulence or shock waves, which would destroy the coherent network. For example, it needs some shelter from the afterflow of high-energy pulsed electrical discharges. Fulgurites provide this in the case of lightning strikes on soils, by the delay of the emerging jet after the shockwave has abated, but this jet may be disturbed by a repeat strike. Thus a ball is more likely from the last strike (also often the longest) down the same path, although the fulgurite may have been formed and well-heated by a previous strike.

It can be seen that the list of requirements above is rather restrictive, and gives some indication of how difficult it is to obtain ball lightning in the laboratory, and indeed in the field. The lack of success in building a ball in the experiments reported here may be caused by something as simple as too much water vapour in the evaporated soil (water was included to prevent soil from fountaining off under the electric field).

13. Conclusions

A physical model of ball lightning is presented which relates it to a normal lightning strike. For a strike on soil (or wood and soil), we point out that chemical reduction of the silicon dioxide component by the carbon component is likely to occur, producing metallic vapour (silicon). Cooling and condensation under chemically reducing conditions after the strike will yield a sparse network of reduced nanoparticles, which is then expected to oxidize, providing the chemical energy for sustained high temperature and the observed radiance. Electronmicrographs are presented of strings of nanospheres sampled and observed after a simulated lightning strike on soil in the lab. A key feature of the model as applied to soils is the penetration below ground level to form a cavity. This enables efficient soil heating by the electrical discharge and provides a delay so the resultant network survives the air disturbance of the lightning. The hot vapour from this cavity erupts back through the opening of the cavity *after the strike*, to form a ring vortex. Formation of nanoparticle networks in the vapour cloud, together with particle charging, then preserves a spherical form, in most cases. It is a consequence of the ring vortex that rotation of any visible internal structure would often be evident.

Detailed time/temperature histories are calculated for a ball of average size 300 mm, and show lifetimes within the range 3–30 s (the commonly observed range) for starting temperatures 1100–1300 K. The model predicts a sudden rise in temperature at the end, to the point where the network melts and disrupts. If network bodies

are formed above *ca.* 1100 K they should be visible from their inception, and will be easily related by an observer to the lightning strike. If less than 1100 K, they could float for minutes, gradually oxidizing and warming until they become visible. These balls would be more difficult for an observer to relate to a previous lightning strike. The model estimates that a simple thermal radiance provides a good match with the observed radiance of an 'average' ball lightning, the common range of colours and with the energy density estimated of the 'average' ball lightning.

Other possible sources of the network ball are lightning strikes on sheet metal structures where a source of carbon such as a rubber seal or plastic window is also vaporized, or man-made electrical discharges to a metal/polymer enclosure. Much higher metal concentrations are expected when the metal vapour is not diluted with hydrocarbon or air, and these may give rise to high-energy ball lightning, much more energetic than the average. The model is consistent with many ball lightning observations, including little change in appearance over the lifetime, and penetration through building materials including glass.

We thank the Electrical and Electronic Engineering Department at the University of Canterbury, New Zealand for the use of their high voltage laboratory, especially Jac Woudberg for his invaluable help in building and operating the capacitor banks over a number of years. Chris Maslin, Bryce Lane, Prin Niamskul, Tim Benson and Alex Simmonds all have written BE research reports preceding and following the experimental work of James Dinniss mainly reported here, with technical help from David Brown, Neville Foot, Ron Boyce and Trevor Berry. Thanks also to Neil Andrews and Jan McKenzie of the Plant and Microbial Sciences Department, and Milo Kral and Mike Flaws of the Mechanical Engineering Department for electronmicroscopy.

Appendix A. Numerical quantities used in the model applied to a soil strike

(*a*) *Ball solids concentration*

For neutral buoyancy, the total mass concentration of particles $C_{\mathrm{tot}} = \rho_{\mathrm{e}} - \rho_{\mathrm{ball}}$. This difference is that between the density of air ρ_{e} surrounding the ball, and the gas (air) within the ball, ρ_{ball}. For temperatures of 300 K for ρ_{e} and 1500 K for ρ_{ball}, $C_{\mathrm{tot}} = 960\ \mathrm{g\,m^{-3}}$. Using the equilibrium calculations of Hutchison *et al.* (1988) (at atmospheric pressure), the mole fraction of Si vapour is 0.2 above Si/O/C mixtures with C/SiO_2 mole ratio around 2 in the temperature range 3000–3500 K. Cooling the gas to 1500 K but with no mixing gives $C_{\mathrm{Si}} = 45\ \mathrm{g\,m^{-3}}$. Added to this is 0.15 mol fraction of SiO vapour, which on *rapid* condensation will bring the reactive solids to *ca.* $100\ \mathrm{g\,m^{-3}}$.

(*b*) *Ball heat release*

The rate of heat release from oxidation equals (enthalpy of formation of SiO_2 from Si_{solid} and O_2) × (linear rate of penetration of oxide layer) × (surface area) × (molar density of Si) equals $790C_{\mathrm{Si}}$ in $\mathrm{W\,m^{-3}}$ of ball volume at 1473 K, for a nanosphere diameter of 25 nm, and C_{Si} in $\mathrm{g\,m^{-3}}$. For a local temperature of T in kelvin, the local rate of heat release $H = 3.17 \times 10^9 (C_{\mathrm{Si}}) \exp(-22\,400/T)$ in $\mathrm{W\,m^{-3}}$, where the activation energy of the reaction is 189 kJ $\mathrm{mol^{-1}}$ (from Deal & Grove 1963, linear rate constant B/A). The rate has been corrected for the O_2 partial pressure, and water vapour partial pressure, so that the base reaction rate is $0.10\ \mathrm{nm\,s^{-1}}$ at 1473 K. For

extended reaction (thick layers), the geometry of the oxide layer becomes important, and may alter the reaction rate compared with that for a flat layer, but the fraction of the nanospheres reacted up to 1700 K has been found to be less than 20%, so this geometry effect has been ignored.

(*c*) *Ball heat loss to surroundings*

The rate of heat loss from the perimeter of the ball is estimated from natural convection from a heated sphere (Bird *et al.* 1960), where the dimensionless Nusselt heat transfer number $Nu = 2 + K(Gr_{\mathrm{D}}Pr)^{1/4}$ for laminar flow around the sphere. Using properties of air at the mean film temperature $(T_{\mathrm{p}} + T_{\mathrm{e}})/2$ to evaluate the Grashof number Gr_{D} and Prandtl number Pr, Nu is found to be 8–10 for a ball diameter of $D = 0.3$ m, and a ball perimeter temperature T_{p} of 1500–1000 K. The total heat loss from the perimeter Q_{p} is then $\pi k D Nu(T_{\mathrm{p}} - T_{\mathrm{e}})$, where k is the conductivity of air in $\mathrm{W\,m^{-1}\,K^{-1}}$ at the film temperature. For a 0.3 m ball with Nu around 9, $Q_{\mathrm{p}} = 8.5k(T_{\mathrm{p}} - 300)$ in watts.

(*d*) *Ball thermal conductivity*

The thermal conductivity of the ball is equated to that of air, which is adequately expressed as a linear function of absolute temperature T, $k = 0.0146 + 5.0 \times 10^{-5}T$ in $\mathrm{W\,m^{-1}\,K^{-1}}$ in the range 500–2000 K.

(*e*) *Ball heat capacity*

The specific heat capacity of the ball per $\mathrm{m^3}$ of volume is $406\,800/T + 0.73C_{\mathrm{tot}}$, where the first term is the air contribution and the second that of the solid content. A total solids content of $900\ \mathrm{g\,m^{-3}}$ is assumed here.

(*f*) *Energy content*

A maximum heat evolution corresponds to all the silicon converting to silica. Thus the calculation limits the total to $32\,915C_{\mathrm{Si}}\ \mathrm{J\,m^{-3}}$.

Appendix B. Factors which can be ignored or must be noted

(*a*) *Diffusion resistance through the interstitial gas*

The centre concentration C_{c} of oxygen can be related easily to the concentration C_{e} at the perimeter of the network ball if one takes the temperature to be uniform through the ball. The diffusivity of oxygen $\boldsymbol{D}$ is then constant, and the rate of consumption of oxygen N_{R} is constant. From an analytical integration of the mass conservation and Fick's law expressions, then $C_{\mathrm{c}} = C_{\mathrm{e}} + N_{\mathrm{R}}R^2/(6\boldsymbol{D})$, where R is the radius of the ball. For $C_{\mathrm{e}} = 8.2\ \mathrm{mol\,m^{-3}}$ (O_2 at 0.2 atm at 300 K), $\boldsymbol{D} = 3 \times 10^{-4}\ \mathrm{m^2\,s^{-1}}$ for oxygen in air at 1500 K, and $N_{\mathrm{R}} = 0.086\ \mathrm{mol\,m^{-3}\,s^{-1}}$ for a mass concentration of silicon metal of $100\ \mathrm{g\,m^{-3}}$ oxidizing at 1473 K, $C_{\mathrm{c}} - C_{\mathrm{e}} = 4.28\ \mathrm{mol\,m^{-3}}$. This is an appreciable drop compared with the available concentration of $8.2\ \mathrm{mol\,m^{-3}}$, so diffusion is expected to limit the reaction somewhat at 1473 K. At a lower temperature of 1400 K, the reaction rate is reduced by a factor 0.344, so $C_{\mathrm{c}} - C_{\mathrm{e}} = 1.47\ \mathrm{mol\,m^{-3}}$. Thus *ca.* 1400 K and below, for a silicon concentration of $100\ \mathrm{g\,m^{-3}}$, diffusion across the ball can be ignored as a limiting factor.

(*b*) *Convective gas flow through the nanoparticle network*

The 'draught pressure difference' across the aerogel ball is due to buoyancy, and the gradient is $(\rho_{\mathrm{e}} - \rho_{\mathrm{ball}})g = (0.96)(9.81) \approx 10\,\mathrm{Pa\,m^{-1}}$. Taking the aerogel as a randomly oriented bed of fibres, each with diameter $d = 25$ nm, and recognizing that the mean free path of the gas is appreciable compared with the fibre diameter, the pressure drop ΔP is related to the superficial velocity v_{s}, viscosity μ and length L by

$$\frac{\Delta P d^2}{L\mu v_{\mathrm{s}}} = 16f\frac{1 + 4\lambda/d}{Ku + (2\lambda/d)(-\ln(f) + f^2/2 - \frac{1}{2})},$$

where Ku is the Kuwabara number (Crawford 1976). Ku is a function of the volumetric fraction f of fibre in the bed, as follows: $Ku = -0.5\ln(f) - 0.75 + f - f^2/4$. For $f = 0.1\,\mathrm{kg\,m^{-3}}/2330\,\mathrm{kg\,m^{-3}} = 4.3 \times 10^{-5}$, $Ku = 4.28$. $\lambda/d = 177\,\mathrm{nm}/25\,\mathrm{nm} = 7.1$ for air at 1500 K. Then the right-hand side equals 1.4×10^{-4}, and the superficial velocity $v_{\mathrm{s}} = 8.2 \times 10^{-7}\,\mathrm{m\,s^{-1}}$. This is negligible, and so the air can be considered to be trapped convectively by the network, and moves wherever it moves.

(*c*) *Heat loss from an individual reacting nanosphere by conductive transfer to the gas within the aerogel*

Considering that the particle has no movement with respect to its surrounding gas, there is no convective heat transfer, and transfer by conduction into a stagnant gas can then be used. A continuum approach gives an order of magnitude result. The Nusselt number $Nu = hd/k = 2$ for this situation (Bird *et al.* 1960), where d is the particle diameter. Substituting in for the heat transfer coefficient $h = Q/(4\pi a^2\Delta T)$, the temperature rise of the particle relative to the gas, $\Delta T = Q/(4\pi ak)$. Using the heat flow Q from the expected reaction rate of a 25 nm diameter sphere of silicon (from above, this is 8.1×10^{-15} W), and thermal conductivity k of air at 1500 K, $\Delta T = 4.7 \times 10^{-7}$ K. This is negligible, so thermal conduction to the surrounding gas is very effective in removing the energy generated in the nanosphere.

(*d*) *Radiation loss from a nanosphere*

We consider radiation losses at 1500 K from nanospheres of silicon, silicon monoxide and silicon dioxide. Black-body radiation (emittance $P_{\mathrm{e}\lambda}$ by the Planck expression) at 1500 K is largely confined to the wavelength range 1–10 µm. The actual emittance is reduced by the factor ε_λ (emissivity), depending on the properties of the particle. For an estimation of radiative loss, we need to integrate the $(\varepsilon_\lambda)(P_{\mathrm{e}\lambda})$ product over the wavelength range of interest. For a single nanosphere of radius a, the total power emitted is

$$W_{\mathrm{p}} = \int 4\pi a^2 \varepsilon_\lambda P_{\mathrm{e}\lambda}\,\mathrm{d}\lambda = 4\pi \int C_{\mathrm{abs}\lambda} P_{\mathrm{e}\lambda}\,\mathrm{d}\lambda,$$

where we have used the equality of emissivity and absorptivity, i.e. $\varepsilon_\lambda = Q_{\mathrm{abs}\lambda} = C_{\mathrm{abs}\lambda}/\pi a^2$, where $C_{\mathrm{abs}\lambda}$ is the absorption cross-section of the particle (Bohren & Huffman 1983). Using the Rayleigh approximation for spheres small compared with the wavelength (i.e. $x = 2\pi a/\lambda \ll 1$, and also $nx \ll 1$),

$$C_{\mathrm{abs}\lambda} = (36\pi(\text{sphere volume})/\lambda)\frac{nk}{(n^2+2)^2},$$

where n and k are the real and imaginary parts, respectively, of the complex refractive index (of the bulk material). For the particle, then $W_p = 9.8\times10^{-21}$ W, 1.2×10^{-18} W and 1.9×10^{-19} W for Si, SiO and SiO_2 nanospheres, respectively. Compared with the chemical release rate, 8.1×10^{-15} W, these are negligible, so radiation is not important for the heat transfer from the nanospheres.

The absorption of any radiation within the aerogel ball depends on the solid volume fraction f, and the linear absorption coefficient

$$\alpha_{\mathrm{abs}\lambda} = \frac{fC_{\mathrm{abs}\lambda}}{(\text{nanosphere volume})}$$

(Bohren & Huffman 1983). Using 100 g Si m^{-3} loading, $f = 4.3 \times 10^{-5}$. The product of $\alpha_{\mathrm{abs}\lambda}R$ is then of the order 0.001 or less, so that the ball is optically transparent in the thermally important wavelengths greater than 1 μm. Thus the radiation from the whole ball can easily be estimated, by simply adding the radiation from all nanospheres in the ball. This comes to 0.000 73 W, 0.088 W and 0.014 W for 300 mm diameter balls of Si, SiO and SiO_2 nanospheres respectively (at 1500 K). These are small compared with the total energy loss rates by convection of *ca.* 20 W. (Note that n and k information for different wavelengths was taken from Palik (1985), with some interpolation for SiO and SiO_2 (cryst.).)

Radiation from the larger, micrometre-sized particles is expected to be no more than in proportion to the masses present (i.e. about eight times), so radiation will still be negligible compared with other means of heat transfer.

References

Abrahamson, J. & Dinniss, J. 2000 Ball lightning caused by oxidation of nanoparticle networks from normal lightning strikes on soil. *Nature* **403**, 519–521.

Abrahamson, J. & Marshall, J. 2002 Permanent electric dipoles on particles leading to filaments in gas-suspensions. *J. Electrostat.* (In the press.)

Abrahamson, J., Bychkov, A. V. & Bychkov, V. L. 2002 Recently reported sightings of ball lightning: observations collected by correspondence and Russian and Ukrainian sightings. *Phil. Trans. R. Soc. Lond.* A **360**, 11–35.

Aleksandrov, V. Ya., Golubev, E. M. & Podmoshenskii, I. V. 1983 Aerosol mode of ball lightning. *Sov. Phys. Tech. Phys.* **27**, 1221–1224.

Andres, U. & Timoshkin, I. 1997 In *IEEE Int. Conf. Conduct. and Breakdown Solid Dielectrics, 22–25 June 1996, Visteris, Sweden*, pp. 452–455.

Andrianov, A. M. & Sinitsyn, V. I. 1977 Erosion-discharge model for ball lightning. *Sov. Phys. Tech. Phys.* **22**, 1342–1347.

Bird, R. B., Stewart, W. E. & Lightfoot, E. N. 1960 *Transport phenomena.* Wiley.

Bohren, C. F. & Huffman, D. R. 1983 *Absorption and scattering of light by small particles.* Wiley.

Brick, R. O. 1968 A method for establishing lightning-resistance/skin-thickness requirements for aircraft. In *Lightning and Static Electricity Conf. Miami Beach, FL, US*, Series AFAL-TR-68-290, vol. 2, pp. 295–317. Dayton, OH: Wright-Patterson Air Force Base.

Bychkov, V. L. 2002 Polymer-composite ball lightning. *Phil. Trans. R. Soc. Lond.* A **360**, 37–60.

Bychkov, A. V., Bychkov, V. L. & Abrahamson, J. 2002 On the energy characteristics of ball lightning. *Phil. Trans. R. Soc. Lond.* A **360**, 97–106.

Chase, M. W., Davies, C. A., Downey, J. R., Frurip, D. J., McDonald, R. A. & Syverud, A. N. 1985 JANAF thermochemical tables, 3rd edn, part II, Cr–Zr. *J. Phys. Chem. Ref. Data* **14**, suppl. no. 1.

Clark, F. M. 1962 *Insulating materials for design and engineering practice*. Wiley.

Crawford, M. 1976 *Air pollution control theory*, pp. 443–444. McGraw-Hill.

Deal, B. E. & Grove, A. S. 1963 General relationship for the thermal oxidation of silicon. *J. Appl. Phys.* **36**, 3770–3778.

Essene, E. J. & Fisher, D. C. 1986 Lightning strike fusion: extreme reduction and metal-silicate liquid immiscibility. *Science* **234**, 189–193.

Fehlner, F. P. & Mott, N. F. 1970 Low-temperature oxidation. *Oxidat. Met.* **2**, 59–99.

Fieux, R., Gary, C. & Hubert, P. 1975 Artificially triggered lightning above land. *Nature* **257**, 212–214.

Fischer, E. 1981 Ball lightning—a combustion phenomenon. *Naturwissenschaften* **68**, 568–569.

Flagan, R. C. & Seinfeld, J. H. 1988 *Fundamentals of air pollution*. Englewood Cliffs, NJ: Prentice-Hall.

Fortov, S. E., Nefedov, A. P., Petrov, O. F., Samaryan, A. A. & Chernyshev, A. V. 1997 Highly nonideal classical thermal plasmas: experimental study of ordered macroparticle structures. *JETP* **84**, 256–261.

Goodlet, B. L. 1937 Lightning. *IEE J.* **81**, 1–56.

Grigor'ev, A. I., Grigor'eva, I. D. & Shiryaeva, S. O. 1992 Ball lightning penetration into closed rooms: 43 eyewitness accounts. *J. Scient. Explorat.* **6**, 261–279.

Hutchison, S. G., Richardson, L. S. & Wai, C. M. 1988 Carbothermic reduction of silicon dioxide—a thermodynamic investigation. *Metall. Trans.* B **19**, 249–253.

Jackson, J. D. 1975 *Classical electrodynamics*, p. 58. Wiley.

Johari, H. 1995 Chemically reactive turbulent vortex rings. *Phys. Fluids* **7**, 2420–2427.

Lamprey, H. & Ripley, R. L. 1962 Ultrafine tungsten and molybdenum powders. *J. Electrochem. Soc.* **109**, 713–716.

Lee, R. H. 1986 The shattering effect of lightning—pressure from heating of air by stroke current. *IEEE Trans. Indust. Applic.* **IA-22**, 416–419.

Littau, K. A., Szajowski, P. J., Muller, A. J., Kortan, A. R. & Brus, L. E. 1993 A luminescent silicon nanocrystal colloid via a high-temperature aerosol reaction. *J. Phys. Chem.* **97**, 1224–1230.

Lowke, J. J., Uman, M. A. & Liebermann, R. W. 1969 Toward a theory of ball lightning. *J. Geophys. Res.* **74**, 6887–6898.

Massoud, H. Z. 1995 The onset of the thermal oxidation of silicon from room temperature to 1000 °C. *Microelectron. Engng* **28**, 109–116.

Massoud, H. Z. & Plummer, J. D. 1987 Analytical relationship for the oxidation of silicon in dry oxygen in the thin-film regime. *J. Appl. Phys.* **62**, 3416–3423.

Merzbacher, C. I. 2002 Materials that emit light by chemical reaction. *Phil. Trans. R. Soc. Lond.* A **360**, 89–96.

Mousa, A. M. 1992 Breakdown gradient of the soil under lightning discharge conditions. In *1992 Int. Aerospace and Ground Conf. on Lightning and Static Electricity, Atlanta City, NJ*, pp. 67-1–67-12.

Nagamori, M., Boivin, J. A. & Claveau, A. 1995 Gibbs free energies of formation of amorphous Si_2O_2. *J. Non-Cryst. Solids* **189**, 270–276.

Olynick, D. L., Gibson, J. M. & Averback, R. S. 1996 Trace oxygen effects on copper nanoparticle size and morphology. *Appl. Phys. Lett.* **68**, 343–345.

Palik, E. D. 1985 *Handbook of optical constants of solids*. Academic.

Pedersen, A. 1989 On the electrical breakdown of gaseous dielectrics. *IEEE Trans. Elect. Insul.* **24**, 721–739.

Pitts, F. L. & Fisher, B. D. 1988 Aircraft jolts from lightning bolts. *IEEE Spectrum* **25**, 34–38.

Rayle, W. D. 1966 Ball lightning characteristics. Note TND-3188. NASA.

Shariff, K. 1992 Vortex rings. *A. Rev. Fluid Mech.* **24**, 235–279.

Siegel, R. W. 1998 In *Physics of new materials*, 2nd edn (ed. F. E. Fujita), pp. 66–106. Springer.

Smirnov, B. M. 1987 The properties and the nature of ball lightning. *Phys. Rep.* **152**, 177–226.

Stokes, A. D. & Cao, L. J. 1989 Ablation arcs. I. Arcs in ice. *J. Phys.* D **22**, 1697–1170.

Stokes, A. D., Sibilski, H. & Kovitya, P. 1989 Ablation arcs. II. Arcs in plastic materials and in boric acid. *J. Phys.* D **22**, 1702–1707.

Stull, D. R. & Prophet, H. 1971 *JANAF thermochemical tables*, 2nd edn. NSRDS-NBS 37. Washington, DC: National Bureau of Standards.

Tepper, F. 1999 Metallic nanopowders produced by the electro-exploding wire process. *Int. J. Powder Metall.* **35**, 39–44.

Turner, D. J. 1994 The structure and stability of ball lightning. *Phil. Trans. R. Soc. Lond.* A **347**, 83–111.

Turner, D. J. 2002 The fragmented science of ball lightning (with comment). *Phil. Trans. R. Soc. Lond.* A **360**, 107–152.

Turner, H. V. & Turner, C. 1973 Phenomena occurring during the extinction of arcs in fuses. In *2nd Int. Symp. on Switching Arc Phenomena*, pp. 253–256.

Xiong, Y. & Pratsinis, S. E. 1993 Formation of agglomerate particles by coagulation and sintering. Part 1. A two-dimensional solution of the population balance equation. *J. Aerosol Sci.* **24**, 283–300.

Yavuz, N. & Can, M. 1999 Experiments on artificial fulgurites under high voltage electrical discharge. *Metallwissen. Technik* **53**, 607–609.